JACS
JOURNAL OF THE AMERICAN CHEMICAL SOCIETY
pubs.acs.org/JACS
Communication

μMap-Red: Proximity Labeling by Red Light Photocatalysis

Benito F. Buksh, Steve D. Knutson, James V. Oakley, Noah B. Bissonnette, Daniel G. Oblinsky, Michael P. Schwoerer, Ciaran P. Seath, Jacob B. Geri, Frances P. Rodriguez-Rivera, Dann L. Parker, Gregory D. Scholes, Alexander Ploss, and David W. C. MacMillan*

Cite This: https://doi.org/10.1021/jacs.2c01384

ABSTRACT: Modern proximity labeling techniques have enabled significant advances in understanding biomolecular interactions. However, current tools primarily utilize activation modes that are incompatible with complex biological environments, limiting our ability to interrogate cell- and tissue-level microenvironments in animal models. Here, we report μMap-Red, a proximity labeling platform that uses a red-light-excited Sn^{IV} chlorin e6 catalyst to activate a phenyl azide biotin probe. We validate μMap-Red by demonstrating photonically controlled protein labeling *in vitro* through several layers of tissue, and we then apply our platform *in cellulo* to label *EGFR* microenvironments and validate performance with STED microscopy and quantitative proteomics. Finally, to demonstrate labeling in a complex biological sample, we deploy μMap-Red in whole mouse blood to profile erythrocyte cell-surface proteins. This work represents a significant methodological advance toward light-based proximity labeling in complex tissue environments and animal models.

Biological processes are regulated by spatial connections between biomolecules, cells, and tissues.[1,2] Understanding these interfaces is key to elucidating the biochemical mechanics of living systems. Significant progress has been made in simple cellular systems, but few technologies can interrogate more complex tissues or animal models. Notably, modern proximity labeling technologies are widely applied for capturing biomolecular interactions in living cells.[3,4] Peroxidase-based approaches, including SPPLAT,[5] EMARS,[6] and APEX,[7] have proven useful in mapping signal transduction networks,[8] tracking subcellular RNA distribution,[9] and delineating synaptic communication.[10] Despite their *in vitro* and simple insect models,[11,12] the use of hydrogen peroxide as a chemical labeling trigger has prohibited their use in more complex systems. Alternatively, biotin ligases[13,14] facilitate labeling in more complex models, including plants[15] and mice,[16] but still require long labeling times (∼18 h) and exhibit poor spatiotemporal control. Protein engineering efforts yielded BASU[17] and TurboID[18] ligases which display faster labeling kinetics, yet these enzymes still suffer from poor control over labeling and exhibit *in vivo* toxicity due to sequestration of endogenous biotin.

Light-based proximity labeling methods have emerged as an attractive alternative because they enable high spatiotemporal control over labeling. Along these lines, we recently developed the μMap photocatalytic labeling strategy for microenvironment mapping, wherein an iridium (Ir) photocatalyst is excited by visible blue light (∼450 nm) to convert nearby diazirines into reactive carbenes via Dexter energy transfer (Figure 1).[19] This platform was successfully employed for a range of applications, including profiling immunosynapse proteins, mapping epigenetic reorganization events,[20] and identifying small-molecule protein targets.[21] More recently, conceptually similar photocatalytic platforms have enabled profiling of cell−cell interactions and the mitochondrial proteome.[22,23] While μMap and other light-based systems offer significant advantages, *in vivo* translation remains a substantial challenge. In particular, shorter-wavelength light (<500 nm) exhibits poor tissue penetration due to scattering effects and absorption overlap with endogenous chromophores.[24] Thus, there remains a significant need to develop labeling platforms that are activated by longer-wavelength light (Figure 1).

In nature, porphyrin and chlorin scaffolds are ubiquitous photocatalysts that absorb longer-wavelength light (>600 nm) and deploy this energy via photoinduced electron transfer. Based upon sporadic reports of azide activation photocatalysts,[25] we reasoned that red-light absorbing catalysts might be used to generate reactive proximity labeling intermediates—nitrenes or aminyl radicals—from aryl azide precursors.[26] We call this red-light-mediated strategy μMap-Red.

To test this idea, we first monitored conversion of 4-azidobenzoic acid (**1**) against several red light photocatalysts with varying redox properties (Figure S1). Using a Sn-metalated chlorin e6 catalyst (**3**), we observed trace conversion (5%) and small quantities of aniline product **2** (2%) (Figure 2a, entry a). An addition of stoichiometric reductants, including glutathione, sodium ascorbate, or NADH led to dramatic yield improvements (Figure 2a, entries b−d), with NADH as the most effective (83% yield). From these data, we propose a mechanistic pathway initiating via reductive quenching of the

Received: February 4, 2022

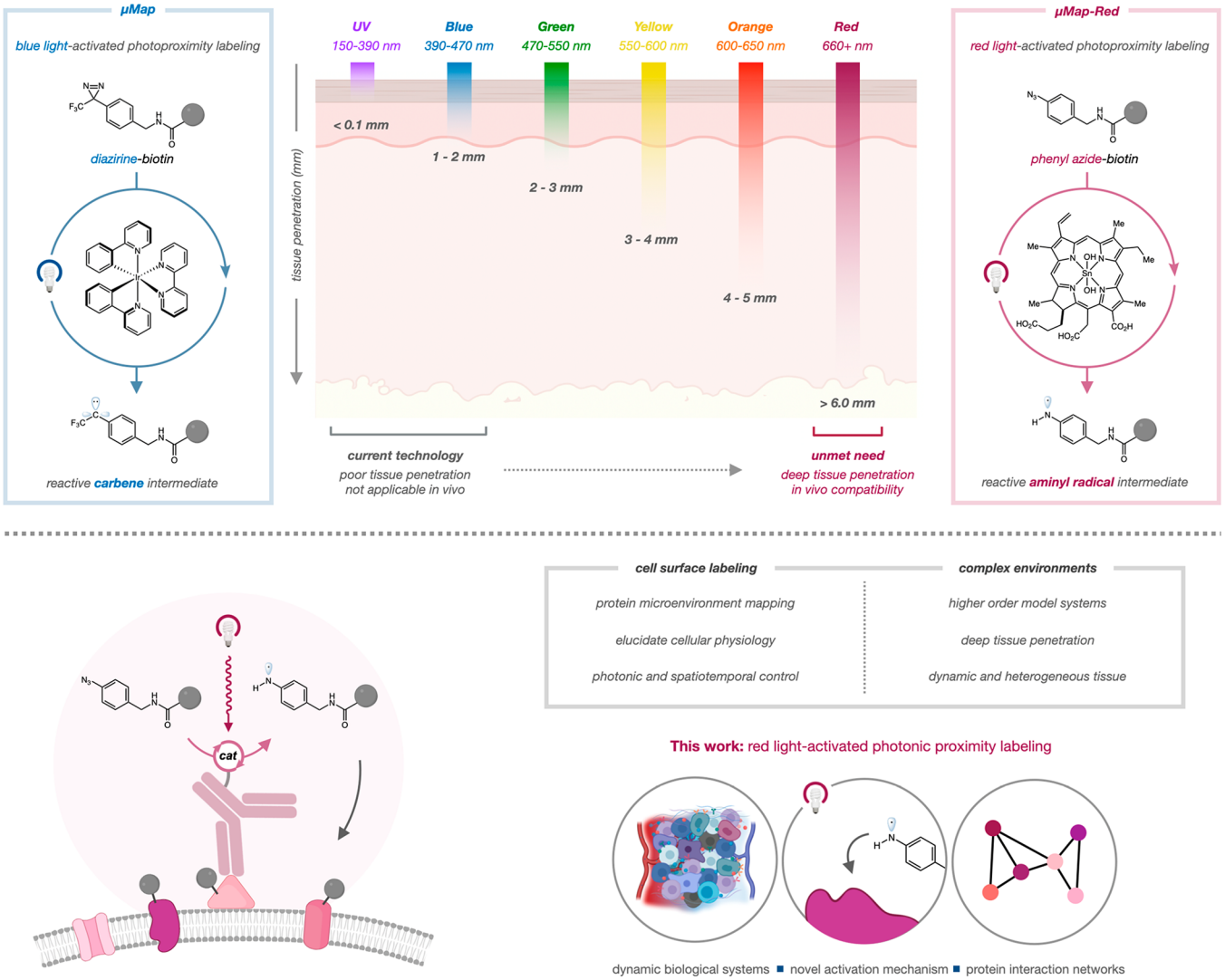

Figure 1. Proximity labeling by red light photoredox catalysis. High-energy light is unable to penetrate tissue, while longer-wavelength light exhibits better penetration. Red-light excitation of Sn−chlorin catalysts can generate reactive aminyl radicals from aryl azides (μMap-Red).

excited-state photocatalyst (**4**) with NADH to form a highly reducing organic ground state ($E_{1/2}$ = −0.69 V vs Ag/AgCl). This reduced species is poised to undergo single electron transfer (SET) to the aryl azide, **1** ($E_{p/2}$ = −0.61 V vs Ag/AgCl), thereby regenerating the catalyst (**3**) (Figure 2b). Mesolytic cleavage of the azide radical anion (**6**) releases molecular nitrogen, and rapid protonation reveals an aminyl radical species (**7**) as a reactive intermediate for proximity labeling. Ultrafast transient-absorption spectroscopy revealed that the excited Sn−chlorin catalyst is quenched by NADH and not by aryl azide **1**, providing support for the proposed ground state reductive electron transfer mechanism (Figure 2c).

Furthermore, electrochemical reduction of the Sn−chlorin e6 catalyst generated a species with significant spectral overlap with the transient-absorption signal of the photoexcited catalyst in the presence of NADH, supporting the generation of the reduced ground state catalyst (Figure S2).

We next sought to validate our platform *in vitro* by covalently tagging a recombinant protein in aqueous solution. We subjected carbonic anhydrase to our optimized labeling conditions (10 mol % catalyst **3**, 1 mM NADH, 500 μM PhN_3-biotin) and were pleased to observe robust protein biotinylation via Western blot (Figure 3a,b). No labeling was observed in the absence of photocatalyst, PhN_3 probe, or light, and labeling intensity was commensurate with increasing irradiation times (Figure S3). Additionally, light dependence on labeling was observed with discrete increases in biotinylation following 2 min pulses of light (Figure 3c). Given our long-term goal of applying this technology for proximity labeling *in vivo*, we probed the efficiency of our system through increasing layers of tissue between the light source and the sample (Figure 3d). Both μMap and μMap-Red protocols achieved robust biotinylation in the absence of tissue obstruction, yet a sharp decrease (~90%) in biotinylation efficiency of μMap was observed with just 1.5 mm of tissue obscuring the light source, confirming poor penetration of blue light through dermal layers.[24] Conversely, μMap-Red exhibited detectable labeling through increasing amounts of tissue (>10 mm) (Figure 3d).

With a system for red-light-activated protein labeling in hand, we next tested μMap-Red in a cellular context. As a model system, we selected epidermal growth factor receptor (*EGFR*), a cell surface receptor-tyrosine kinase. We first synthesized secondary antibodies conjugated to Sn−chlorin, which could then be directed with primary antibodies to *EGFR* (Figure 4a).

https://doi.org/10.1021/jacs.2c01384
J. Am. Chem. Soc. XXXX, XXX, XXX−XXX

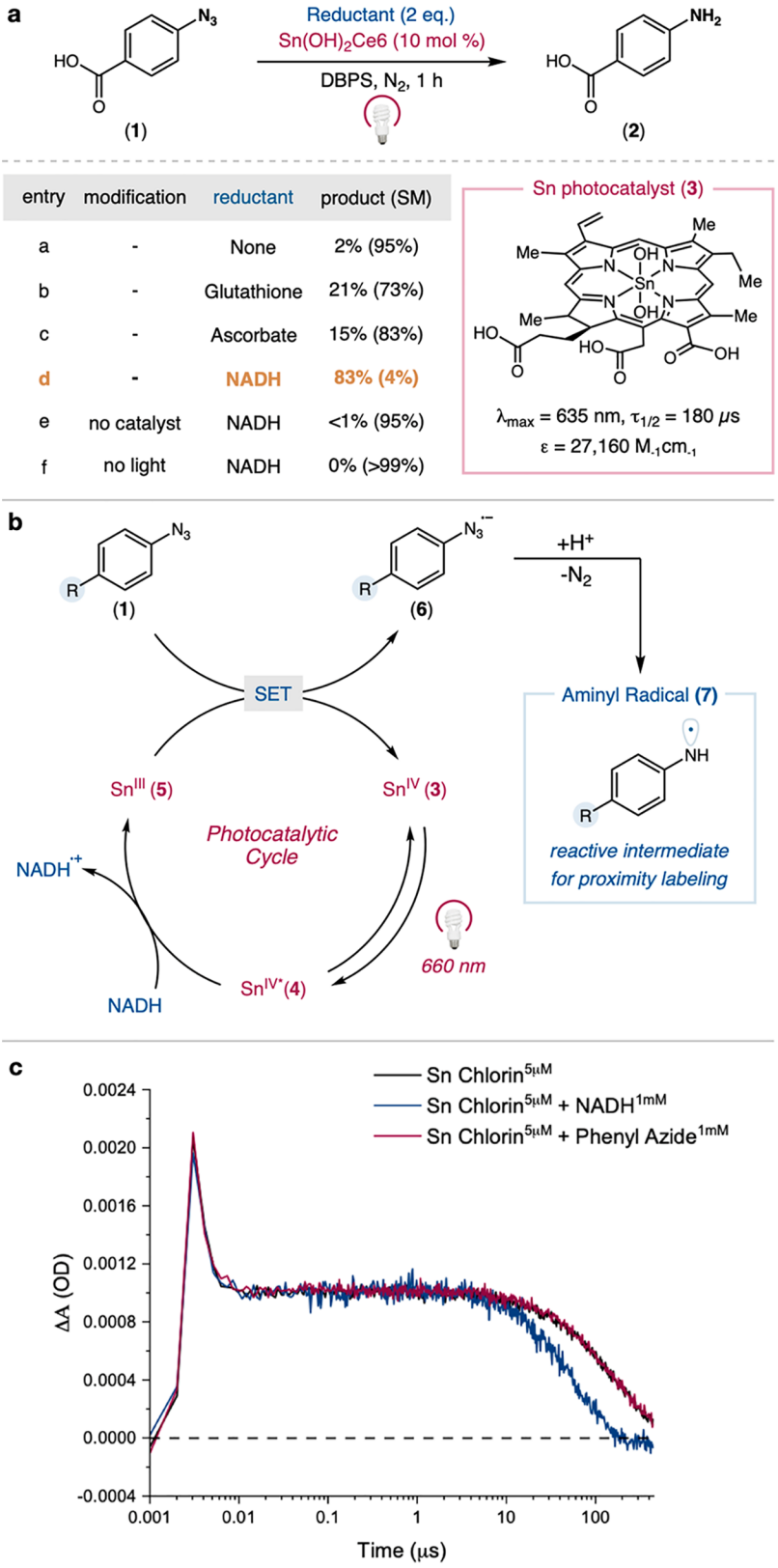

Figure 2. Reaction optimization, proposed mechanism, and transient absorption spectroscopy. (a) Effect of reductant on phenyl azide conversion using catalyst **3**. (b) Proposed reaction mechanism. (c) Time-resolved transient absorption spectroscopy of $Sn(OH)_2$–chlorin e6 in the presence of phenyl azide **1** or NADH.

We subjected A549 cells to immunotargeted photolabeling (1 mM NADH, 500 μM PhN_3-biotin, 30 min irradiation) in the presence or absence of anti-*EGFR* antibodies. Spatially selective biotinylation was assessed via stimulated emission depletion (STED) super-resolution microscopy. Gratifyingly, μMap-Red exhibited robust cell-surface biotinylation only in the presence of

https://doi.org/10.1021/jacs.2c01384
J. Am. Chem. Soc. XXXX, XXX, XXX−XXX

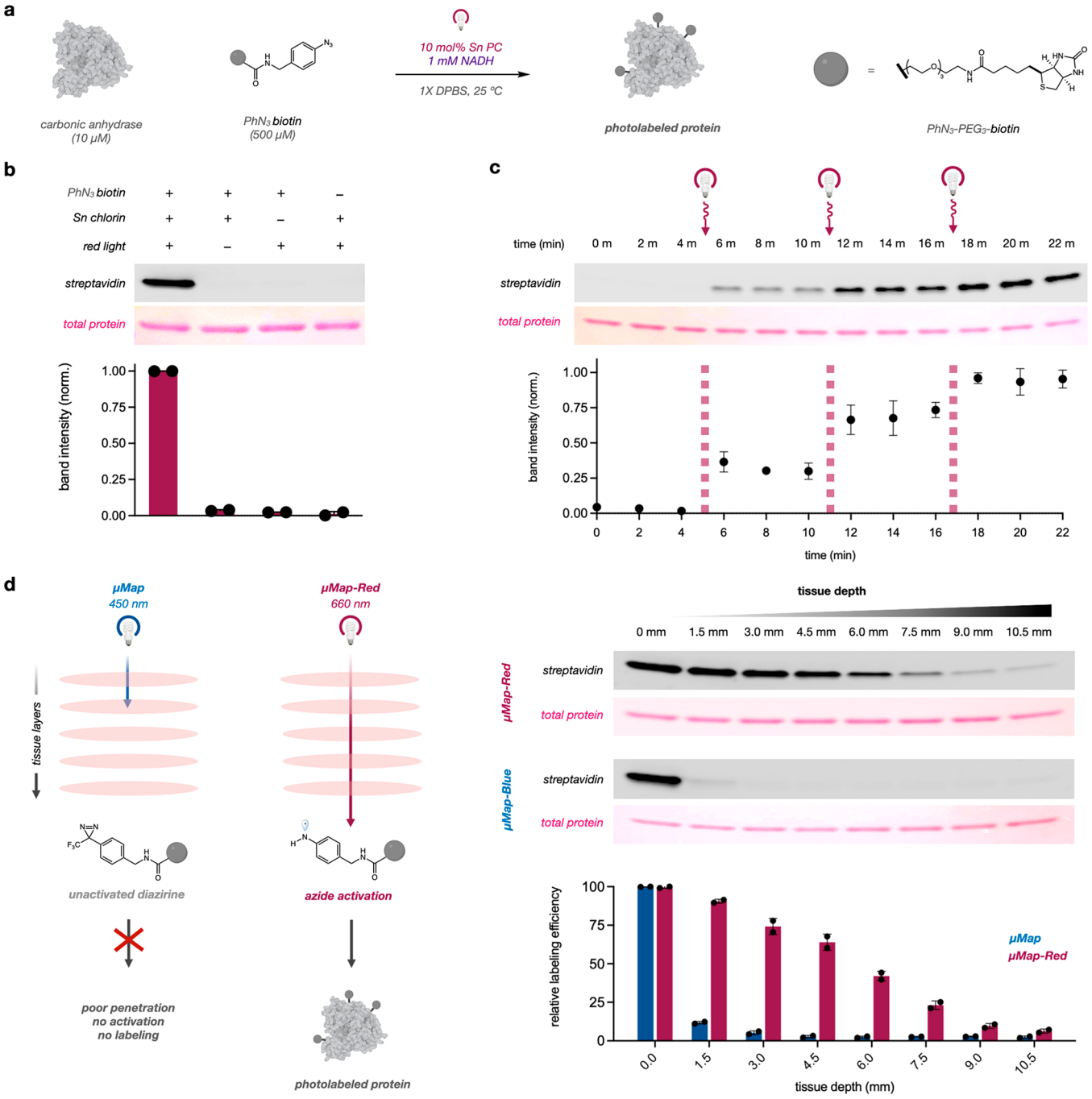

Figure 3. μMap-Red enables photonically controlled protein labeling and penetrates tissue layers. (a) Scheme for protein biotinylation and (b) relevant reaction controls. Bars and data points represent normalized densitometric measurements from two separate experiments, and error bars denote standard error. (c) Photonic control over protein biotinylation. A labeling reaction was prepared, and aliquots were taken every 2 min. Samples were irradiated with red light for 2 min at 4, 10, and 16 min time points. (d) μMap-Red and μMap labeling through tissue. Labeling reactions were illuminated under red or blue light, and increasing slices of raw meat were inserted between reactions and light sources. All *in vitro* reactions were analyzed via Western blot.

anti-*EGFR* antibodies, indicating low nonspecific binding or off-target labeling (Figure 4b). The high resolution offered by STED microscopy also allowed us to qualitatively assess colocalization of *EGFR* and labeling. As shown in Figure 4b, we observed a biotinylation signal that strongly overlaid with *EGFR* staining, signifying confinement of labeling to the *EGFR* microenvironment. To assess spatial selectivity of labeling, a measurement of the full width at half-maximum (fwhm) of biotinylation clusters estimated the Gaussian distribution of labeling events to be 87 ± 33 nm (n = 50 clusters) (Figure S20). This distribution is in agreement with the known longer lifetime of the aminyl radical intermediate (~50 μs)[27] with respect to carbenes (~2 ns) generated using μMap[19] but nonetheless affords μMap-Red with the ability to profile nanoscale events in individual protein microenvironments.

We next generated membrane lysate fractions from photolabeled cells and subjected them to streptavidin enrichment and quantitative proteomics. Consistent with our STED analysis, we

https://doi.org/10.1021/jacs.2c01384
J. Am. Chem. Soc. XXXX, XXX, XXX−XXX

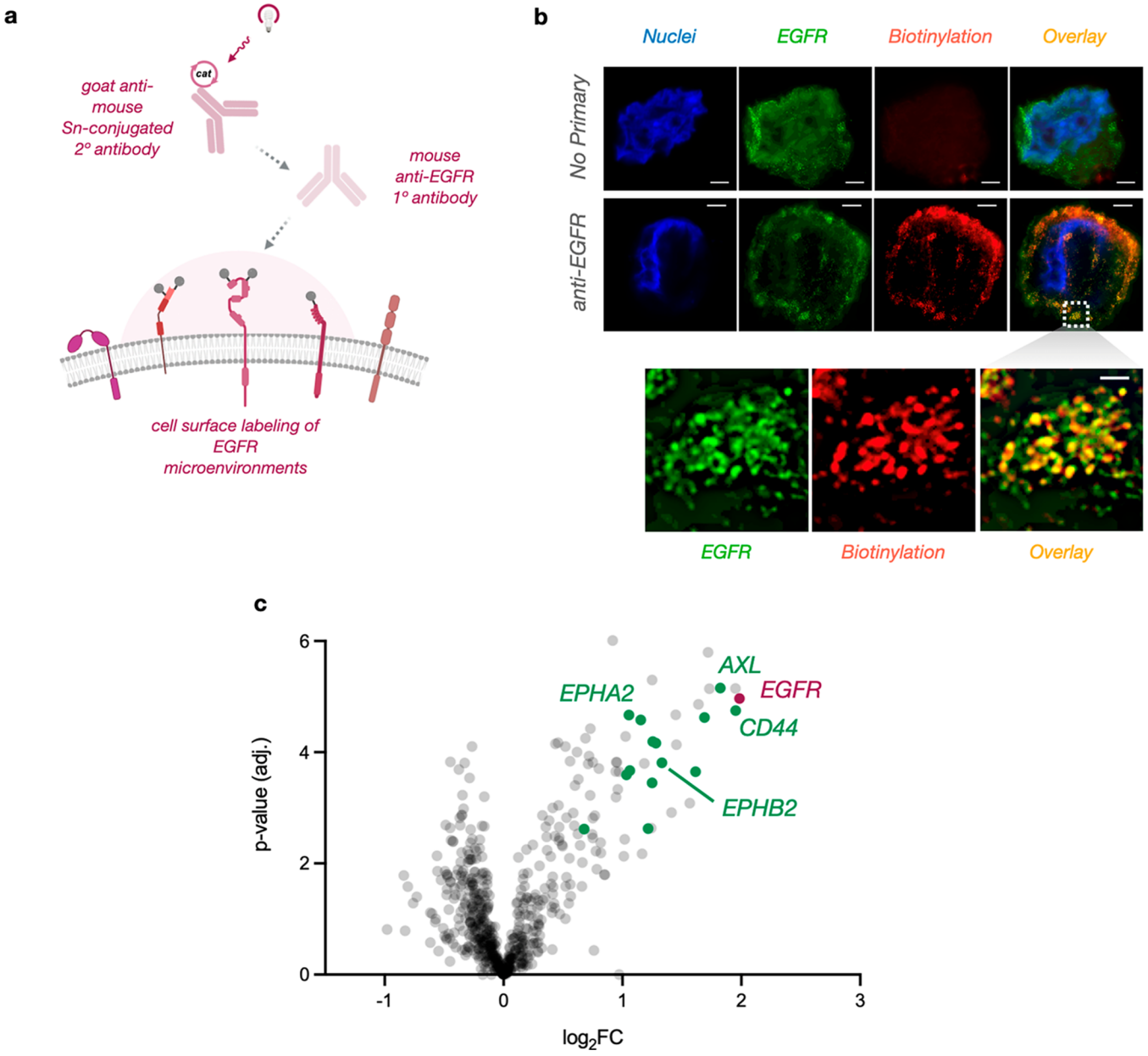

Figure 4. μMap-Red photolabels cell-surface receptor microenvironments on living cells. (a) Primary anti-*EGFR* antibodies and Sn-conjugated secondary antibodies were used to label microenvironments on living A549 cells. (b) STED microscopy of photolabeled cells with and without anti-*EGFR* primary antibodies. The inset represents a magnified region of interest illustrating radial labeling clusters overlaid with individual *EGFR* protein microenvironments. Depicted scale bar is 2 μm for no primary, 3 μm for anti-EGFR, and 1 μm for the zoomed inset. (c) Quantitative proteomics volcano plot of enriched proteins. Green data points represent known *EGFR* interactors from the BioGrid database.[28]

observed *EGFR* enrichment via Western blot only in samples that had been exposed to anti-*EGFR* antibody (Figure S4). Here, quantitative tandem mass tag (TMT) proteomics revealed 29 enriched proteins with $\log_2(\mathrm{FC}) > 1$ (Figure 4c). Satisfyingly, *EGFR* was the most enriched protein in the data set. Of these enriched proteins, 12 have previously validated physical interactions with *EGFR* (Figure 4c, green data points),[28] including *CD44*, a transmembrane glycoprotein known to regulate *EGFR* autophosphorylation.[29] Additionally, one of the most enriched proteins, *AXL*, is a known substrate of *EGFR* phosphorylation.[30] *EPHA2* and *EPHB2*, also receptor protein-tyrosine kinases, were highly enriched in our data set and are known to modulate vesicular trafficking of *EGFR*.[31] Together, these data validate the accuracy of μMap-Red as a proximity labeling platform for profiling spatial connections in signaling pathways.

We next sought to evaluate our platform in a complex setting where blue light activation would not be feasible. Along these lines, whole blood presents high levels of biochemical complexity, and we questioned whether μMap-Red could be used in this setting to achieve selective proximity labeling. We selected TER119, a well-characterized antibody raised against mature erythrocytes,[32] as our targeting modality for cell-surface labeling (Figure 5). Interestingly, although TER119 is monoclonal, it has been shown to bind several targets on red blood cells and remains a gold standard erythrocyte marker for flow cytometry analysis of whole blood.[33] First, we conjugated Sn−chlorin catalysts to both TER119 and a nontargeting isotype

https://doi.org/10.1021/jacs.2c01384
J. Am. Chem. Soc. XXXX, XXX, XXX−XXX

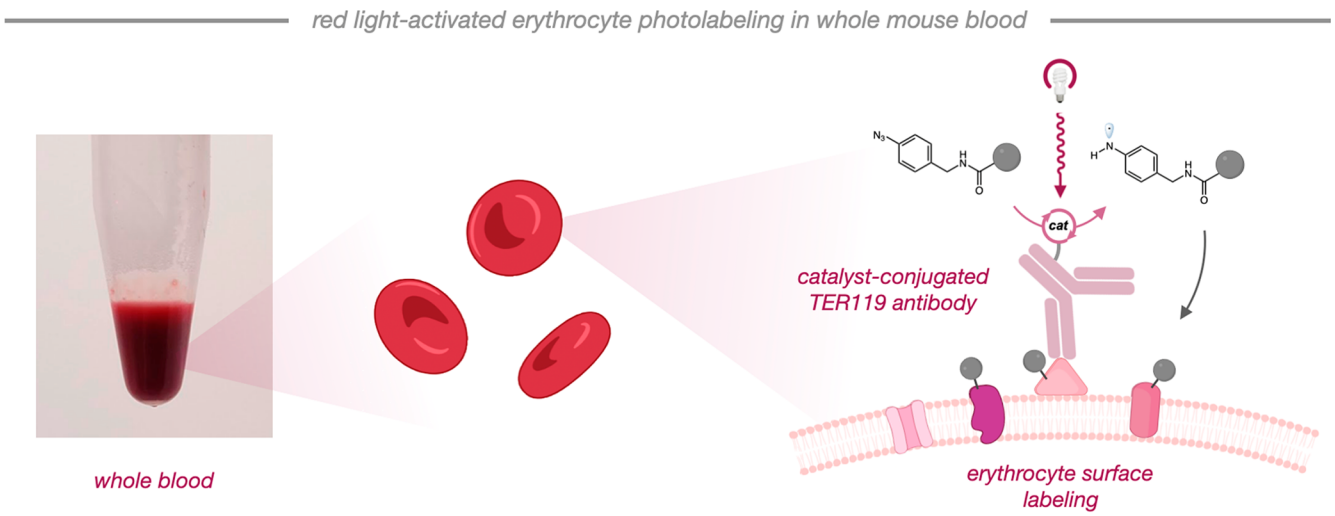

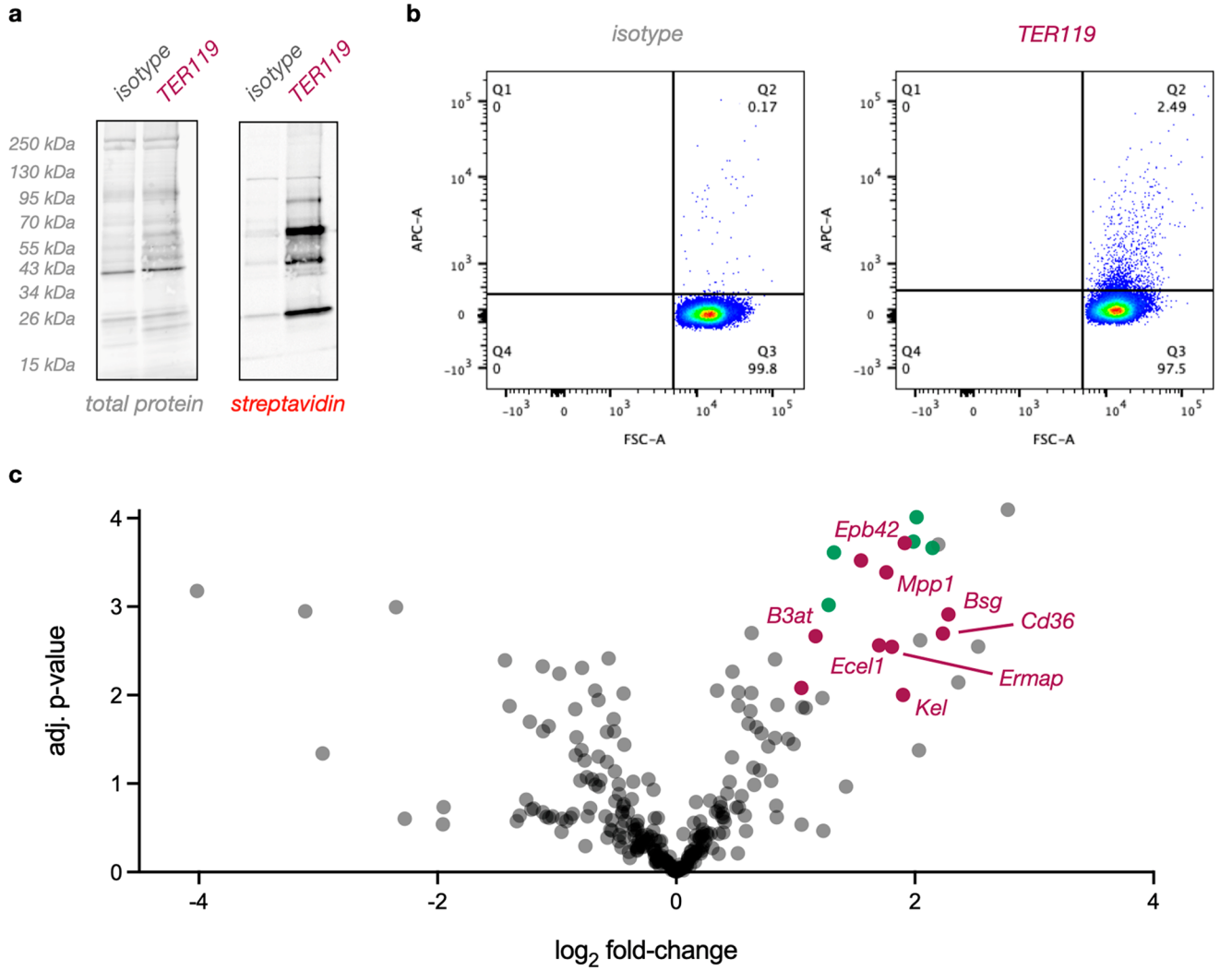

Figure 5. μMap-Red profiles erythrocyte surface proteins in whole mouse blood. (top) Scheme for biotinylation of erythrocyte surfaces in whole blood. (a) Western blot analysis of erythrocyte membrane lysate from isotype and TER119-directed photolabeling. (b) Flow cytometry of isotype or TER119 photolabeled cells. (c) Quantitative proteomics volcano plot of identified proteins after whole blood photolabeling. Red data points represent known erythrocyte membrane proteins while green points denote integral membrane-associated proteins.

control. We then added these conjugates, along with the μMap-Red reaction components—1 mM NADH and 500 μM PhN_3-biotin—directly to samples of whole mouse blood. Following a 1 h incubation period, samples were irradiated for 10 min, and membrane lysates were collected. Strikingly, biotinylation via Western blot analysis was only observed with the catalyst-

https://doi.org/10.1021/jacs.2c01384
J. Am. Chem. Soc. XXXX, XXX, XXX−XXX

conjugated TER119, and minimal signal was observed with isotype conjugates (Figure 5a). Intensity of labeling was proportional to TER119 concentration while no biotinylation was observed with any amount of isotype (Figure 5a, Figure S5). Remarkably, we repeated this experiment using blue-light-activated μMap and observed no signal across all conditions (Figure S6), consistent with the observed poor tissue penetration of blue light (Figure 3d). In parallel, we analyzed photolabeled blood via flow cytometry by staining with fluorescent Neutravidin-DyLight 650. As shown in Figure 5b, minimal signal was observed in the isotype reactions, while a significant (~15-fold) increase in biotinylated cells was seen with TER119 reactions, indicating erythrocyte labeling in whole blood. Finally, we performed quantitative proteomics on enriched membrane lysates (Figure 5c). We observed 24 proteins that were strongly enriched [$\log_2$(FC) > 1] in our data set, the majority of which are known erythrocyte cell surface proteins (Figure 5C, red data points). In particular, basigin (*Bsg*), *Cd36*, *Kel*, erythrocyte membrane associated protein (*Ermap*), 55 kDa erythrocyte membrane protein (*Mpp1*), band 3 anion transport protein (*B3at*), and protein 4.2 (*Epb42*) were among the most enriched. These targets constitute the major mouse erythrocyte membrane proteins and blood antigen group glycoproteins and likely represent the major TER119 antigen ensemble.[34] Additionally, we observed enrichment of several cytoskeletal proteins (Figure 5C, green data points), including spectrins alpha and beta as well as ankyrin and alpha-adducin.[35]

In conclusion, we disclose here a novel red-light-activated proximity labeling platform. We show that this system exhibits phototonic and spatiotemporal control over labeling and can operate in both simple and complex biological environments. Although μMap-Red enables robust photoproximity labeling through tissue and in whole blood, challenges remain for translating this platform into living animals. While azides have been utilized for biorthogonal conjugation in worms, zebrafish, and mice,[36,37] significant pharmacokinetic optimization of photocatalyst, probe, and reductant delivery is required for translation into organismal contexts. Additionally, minimizing reactive oxygen species generation, phototoxicity, and local tissue heating will be key parameters for successful *in vivo* applications. Together, this methodology represents a significant advance toward developing red-light-activated labeling platforms for elucidating spatial interactomes in animal models.

■ ASSOCIATED CONTENT

Supporting Information

The Supporting Information is available free of charge at https://pubs.acs.org/doi/10.1021/jacs.2c01384.

Proteomic data sets (XLSX)

Experimental procedures, characterization data, and supplementary figures (PDF)

■ AUTHOR INFORMATION

Corresponding Author

David W. C. MacMillan − *Merck Center for Catalysis at Princeton University, Princeton, New Jersey 08544, United States; Department of Chemistry, Princeton University, Princeton, New Jersey 08544, United States;* orcid.org/0000-0001-6447-0587; Email: dmacmill@princeton.edu

Authors

Benito F. Buksh − *Merck Center for Catalysis at Princeton University, Princeton, New Jersey 08544, United States; Department of Chemistry, Princeton University, Princeton, New Jersey 08544, United States*

Steve D. Knutson − *Merck Center for Catalysis at Princeton University, Princeton, New Jersey 08544, United States; Department of Chemistry, Princeton University, Princeton, New Jersey 08544, United States*

James V. Oakley − *Merck Center for Catalysis at Princeton University, Princeton, New Jersey 08544, United States; Department of Chemistry, Princeton University, Princeton, New Jersey 08544, United States*

Noah B. Bissonnette − *Merck Center for Catalysis at Princeton University, Princeton, New Jersey 08544, United States; Department of Chemistry, Princeton University, Princeton, New Jersey 08544, United States;* orcid.org/0000-0001-6892-5040

Daniel G. Oblinsky − *Department of Chemistry, Princeton University, Princeton, New Jersey 08544, United States;* orcid.org/0000-0001-7460-8260

Michael P. Schwoerer − *Department of Molecular Biology, Princeton University, Princeton, New Jersey 08544, United States*

Ciaran P. Seath − *Merck Center for Catalysis at Princeton University, Princeton, New Jersey 08544, United States; Department of Chemistry, Princeton University, Princeton, New Jersey 08544, United States*

Jacob B. Geri − *Merck Center for Catalysis at Princeton University, Princeton, New Jersey 08544, United States; Department of Chemistry, Princeton University, Princeton, New Jersey 08544, United States*

Frances P. Rodriguez-Rivera − *Discovery Chemistry, Merck & Co., Kenilworth, New Jersey 07033, United States;* orcid.org/0000-0003-0651-8639

Dann L. Parker − *Discovery Chemistry, Merck & Co., Kenilworth, New Jersey 07033, United States*

Gregory D. Scholes − *Department of Chemistry, Princeton University, Princeton, New Jersey 08544, United States;* orcid.org/0000-0003-3336-7960

Alexander Ploss − *Department of Molecular Biology, Princeton University, Princeton, New Jersey 08544, United States;* orcid.org/0000-0001-9322-7252

Complete contact information is available at: https://pubs.acs.org/10.1021/jacs.2c01384

Notes

The authors declare the following competing financial interest(s): A provisional U.S. patent has been filed by D.W.C.M., J.B.G., and B.F.B. based in part on this work, 63/076,099; 63/252,244. International Application No. PCT/US2021/019959. D.W.C.M. declares an ownership interest in Penn PhD, which has commercialized materials used in this work.

■ ACKNOWLEDGMENTS

This work was funded by the NIH National Institute of General Medical Sciences (R35-GM134897-02) and kind gifts from Merck, BMS, Pfizer, Janssen, Genentech, and Eli Lilly. We also acknowledge the Princeton Catalysis Initiative for supporting this work. S.D.K. acknowledges the NIH for a postdoctoral fellowship (1F32GM142206-01). J.V.O. acknowledges the

National Science Foundation Graduate Research Fellowship Program (DGE-1656466). Mechanistic experiments, including transient absorption and UV−vis spectroscopy, were supported by the Division of Chemical Sciences, Geosciences, and Biosciences, Office of Basic Energy Sciences of the U.S. Department of Energy (DOE) through grant DE-SC0019370. M.P.S. is supported by the NIGMS of the National Institutes of Health under Grant T32GM007388 and a HMEI-STEP fellowship from the from the High Meadows Environmental Institute at Princeton University. Imaging was performed with support from the Confocal Imaging Facility, a Nikon Center of Excellence, in the Department of Molecular Biology at Princeton University. The authors thank Saw Kyin and Henry H. Shwe at the Princeton Proteomics Facility. We thank Christina DeCoste, Katherine Rittenbach, and the Princeton University Molecular Biology Flow Cytometry Resource Facility which is partially supported by the Cancer Institute of New Jersey Cancer Center Support Grant (P30CA072720). Generalized schemes were created using Biorender.

REFERENCES

(1) Keskin, O.; Tuncbag, N.; Gursoy, A. Predicting protein−protein interactions from the molecular to the proteome level. *Chem. Rev.* **2016**, *116* (8), 4884−4909.
(2) Hentze, M. W.; Castello, A.; Schwarzl, T.; Preiss, T. A brave new world of RNA-binding proteins. *Nat. Rev. Mol. Cell. Biol.* **2018**, *19* (5), 327−341.
(3) Qin, W.; Cho, K. F.; Cavanagh, P. E.; Ting, A. Y. Deciphering molecular interactions by proximity labeling. *Nat. Methods* **2021**, *18* (2), 133−143.
(4) Seath, C. P.; Trowbridge, A. D.; Muir, T. W.; MacMillan, D. W. Reactive intermediates for interactome mapping. *Chem. Soc. Rev.* **2021**, *50*, 2911−2926.
(5) Rees, J. S.; Li, X. W.; Perrett, S.; Lilley, K. S.; Jackson, A. P. Selective proteomic proximity labeling assay using tyramide (SPPLAT): a quantitative method for the proteomic analysis of localized membrane-bound protein clusters. *Curr. Protoc. Protein Sci.* **2017**, *88* (1), 19.27.1−19.27.18.
(6) Honke, K.; Kotani, N. The enzyme-mediated activation of radical source reaction: a new approach to identify partners of a given molecule in membrane microdomains. *J. Neurochem.* **2011**, *116* (5), 690−695.
(7) Lam, S. S.; Martell, J. D.; Kamer, K. J.; Deerinck, T. J.; Ellisman, M. H.; Mootha, V. K.; Ting, A. Y. Directed evolution of APEX2 for electron microscopy and proximity labeling. *Nat. Methods* **2015**, *12* (1), 51−54.
(8) Liu, G.; Papa, A.; Katchman, A. N.; Zakharov, S. I.; Roybal, D.; Hennessey, J. A.; Kushner, J.; Yang, L.; Chen, B.-X.; Kushnir, A. Mechanism of adrenergic Ca V 1.2 stimulation revealed by proximity proteomics. *Nature* **2020**, *577* (7792), 695−700.
(9) Fazal, F. M.; Han, S.; Parker, K. R.; Kaewsapsak, P.; Xu, J.; Boettiger, A. N.; Chang, H. Y.; Ting, A. Y. Atlas of subcellular RNA localization revealed by APEX-seq. *Cell* **2019**, *178* (2), 473−490.
(10) Martell, J. D.; Yamagata, M.; Deerinck, T. J.; Phan, S.; Kwa, C. G.; Ellisman, M. H.; Sanes, J. R.; Ting, A. Y. A split horseradish peroxidase for the detection of intercellular protein−protein interactions and sensitive visualization of synapses. *Nat. Biotechnol.* **2016**, *34* (7), 774−780.
(11) Reinke, A. W.; Mak, R.; Troemel, E. R.; Bennett, E. J. In vivo mapping of tissue-and subcellular-specific proteomes in Caenorhabditis elegans. *Sci. Adv.* **2017**, *3* (5), No. e1602426.
(12) Mannix, K. M.; Starble, R. M.; Kaufman, R. S.; Cooley, L. Proximity labeling reveals novel interactomes in live Drosophila tissue. *Development* **2019**, *146* (14), dev176644.
(13) Choi-Rhee, E.; Schulman, H.; Cronan, J. E. Promiscuous protein biotinylation by Escherichia coli biotin protein ligase. *Protein Sci.* **2004**, *13* (11), 3043−3050.
(14) Roux, K. J.; Kim, D. I.; Raida, M.; Burke, B. A promiscuous biotin ligase fusion protein identifies proximal and interacting proteins in mammalian cells. *J. Cell Biol.* **2012**, *196* (6), 801−810.
(15) Khan, M.; Youn, J.-Y.; Gingras, A.-C.; Subramaniam, R.; Desveaux, D. In planta proximity dependent biotin identification (BioID). *Sci. Rep.* **2018**, *8* (1), 1−8.
(16) Uezu, A.; Kanak, D. J.; Bradshaw, T. W.; Soderblom, E. J.; Catavero, C. M.; Burette, A. C.; Weinberg, R. J.; Soderling, S. H. Identification of an elaborate complex mediating postsynaptic inhibition. *Science* **2016**, *353* (6304), 1123−1129.
(17) Ramanathan, M.; Majzoub, K.; Rao, D. S.; Neela, P. H.; Zarnegar, B. J.; Mondal, S.; Roth, J. G.; Gai, H.; Kovalski, J. R.; Siprashvili, Z. RNA−protein interaction detection in living cells. *Nat. Methods* **2018**, *15* (3), 207.
(18) Branon, T. C.; Bosch, J. A.; Sanchez, A. D.; Udeshi, N. D.; Svinkina, T.; Carr, S. A.; Feldman, J. L.; Perrimon, N.; Ting, A. Y. Efficient proximity labeling in living cells and organisms with TurboID. *Nat. Biotechnol.* **2018**, *36* (9), 880−887.
(19) Geri, J. B.; Oakley, J. V.; Reyes-Robles, T.; Wang, T.; McCarver, S. J.; White, C. H.; Rodriguez-Rivera, F. P.; Parker, D. L.; Hett, E. C.; Fadeyi, O. O.; Oslund, R. C.; MacMillan, D. W. Microenvironment mapping via Dexter energy transfer on immune cells. *Science* **2020**, *367* (6482), 1091−1097.
(20) Seath, C. P.; Burton, A. J.; MacMillan, D. W.; Muir, T. W.Tracking chromatin state changes using μMap photo-proximity labeling. *bioRxiv*, 2021. https://doi.org/10.1101/2021.09.28.462236 (accessed 2022-03-24).
(21) Trowbridge, A. D.; Seath, C. P.; Rodriguez-Rivera, F. P.; Li, B. X.; Dul, B. E.; Schwaid, A. G.; Geri, J. B.; Oakley, J. V.; Fadeyi, O. O.; Oslund, R. C.; et al.Small molecule photocatalysis enables drug target identification via energy transfer. *bioRxiv*, 2021. https://doi.org/10.1101/2021.08.02.454797 (accessed 2022-03-24).
(22) Oslund, R. C.; Reyes-Robles, T.; White, C. H.; Tomlinson, J. H.; Crotty, K. A.; Bowman, E. P.; Chang, D.; Peterson, V. M.; Li, L.; Frutos, S.; et al.Detection of Cell-Cell Interactions via Photocatalytic Cell Tagging. *bioRxiv*, 2021. https://doi.org/10.1101/2021.10.04.463039 (accessed 2022-03-24).
(23) Wang, H.; Zhang, Y.; Zeng, K.; Qiang, J.; Cao, Y.; Li, Y.; Fang, Y.; Zhang, Y.; Chen, Y. Selective Mitochondrial Protein Labeling Enabled by Biocompatible Photocatalytic Reactions inside Live Cells. *JACS Au* **2021**, *1*, 1066−1075.
(24) Ash, C.; Dubec, M.; Donne, K.; Bashford, T. Effect of wavelength and beam width on penetration in light-tissue interaction using computational methods. *Lasers Medical Sci.* **2017**, *32* (8), 1909−1918.
(25) Leyshon, L. J.; Reiser, A. Sensitized photodecomposition of phenyl azide and α-naphthyl azide. *J. Chem. Soc., Faraday Trans. 2* **1972**, *68* (0), 1918−1927.
(26) Our group submitted a provisional patent (No. 63/076,099) on this technology on 09/09/2020. Later, during the preparation of this manuscript, a conceptually similar technology was published as a preprint: Tay, N.; Ryu, K. A.; Weber, J.; Olow, A.; Reichman, D.; Oslund, R.; Fadeyi, O.; Rovis, T.Targeted Activation in Localized Protein Environments via Deep Red Photoredox Catalysis. *chemRxiv*, 2021. https://doi.org/10.26434/chemrxiv-2021-x9bjv (accessed 2022-03-24).
(27) Wagner, B. D.; Ruel, G.; Lusztyk, J. Absolute Kinetics of Aminium Radical Reactions with Olefins in Acetonitrile Solution1. *J. Am. Chem. Soc.* **1996**, *118* (1), 13−19.
(28) Stark, C.; Breitkreutz, B.-J.; Reguly, T.; Boucher, L.; Breitkreutz, A.; Tyers, M. BioGRID: a general repository for interaction datasets. *Nucleic Acids Res.* **2006**, *34* (1), D535−D539.
(29) Perez, A.; Neskey, D. M.; Wen, J.; Pereira, L.; Reategui, E. P.; Goodwin, W. J.; Carraway, K. L.; Franzmann, E. J. CD44 interacts with EGFR and promotes head and neck squamous cell carcinoma initiation and progression. *Oral Oncol.* **2013**, *49* (4), 306−313.
(30) Vouri, M.; Croucher, D.; Kennedy, S.; An, Q.; Pilkington, G.; Hafizi, S. Axl-EGFR receptor tyrosine kinase hetero-interaction provides EGFR with access to pro-invasive signalling in cancer cells. *Oncogenesis* **2016**, *5* (10), e266−e266.

https://doi.org/10.1021/jacs.2c01384
J. Am. Chem. Soc. XXXX, XXX, XXX−XXX

(31) Stallaert, W.; Brüggemann, Y.; Sabet, O.; Baak, L.; Gattiglio, M.; Bastiaens, P. I. Contact inhibitory Eph signaling suppresses EGF-promoted cell migration by decoupling EGFR activity from vesicular recycling. *Sci. Signal.* **2018**, *11* (541), No. eaat0114.
(32) Ikuta, K.; Kina, T.; MacNeil, I.; Uchida, N.; Peault, B.; Chien, Y.-h.; Weissman, I. L. A developmental switch in thymic lymphocyte maturation potential occurs at the level of hematopoietic stem cells. *Cell* **1990**, *62* (5), 863−874.
(33) Kina, T.; Ikuta, K.; Takayama, E.; Wada, K.; Majumdar, A. S.; Weissman, I. L.; Katsura, Y. The monoclonal antibody TER-119 recognizes a molecule associated with glycophorin A and specifically marks the late stages of murine erythroid lineage. *Br. J. Hamaetol.* **2000**, *109* (2), 280−287.
(34) Pasini, E. M.; Kirkegaard, M.; Salerno, D.; Mortensen, P.; Mann, M.; Thomas, A. W. Deep coverage mouse red blood cell proteome. *Mol. Cell. Proteomics* **2008**, *7* (7), 1317−1330.
(35) Peng, Z.; Li, X.; Pivkin, I. V.; Dao, M.; Karniadakis, G. E.; Suresh, S. Lipid bilayer and cytoskeletal interactions in a red blood cell. *Proc. Natl. Acad. Sci. U. S. A.* **2013**, *110* (33), 13356−13361.
(36) Sletten, E. M.; Bertozzi, C. R. From mechanism to mouse: a tale of two bioorthogonal reactions. *Acc. Chem. Res.* **2011**, *44* (9), 666−676.
(37) Chang, P. V.; Prescher, J. A.; Sletten, E. M.; Baskin, J. M.; Miller, I. A.; Agard, N. J.; Lo, A.; Bertozzi, C. R. Copper-free click chemistry in living animals. *Proc. Natl. Acad. Sci. U. S. A.* **2010**, *107* (5), 1821−1826.

https://doi.org/10.1021/jacs.2c01384
J. Am. Chem. Soc. XXXX, XXX, XXX−XXX